

Journal of Materials and Engineering Structures

Research Paper

Investigation of Bending Response in Hollow Core Beams: Experimental and Analytical Insights

Jagruti S. Nikam [a,*], Abhijit J. Pawar [a]

[a] *Department of Civil Engineering, K K Wagh Institute of Engineering Education and Research, Nashik 422003, Maharashtra, India*

ARTICLE INFO

Article history :

Received : 29 September 2025

Revised : 4 December 2025

Accepted : 17 February 2026

Keywords:

hollow core beam

flexural behavior

two-point loading

finite element analysis

ABSTRACT

The idea of using hollow cores in bridges is quite common, but it can be effectively applied to reinforced concrete beams in RCC buildings. The major advantage of use hollow cores is the reduction in the overall self-weight of the beam. This leads to a lower dead load on columns and foundations, which may help to cut down the amount of concrete and steel needed—making the structure more economical. While many researchers have investigated the structural behavior of hollow core beams under flexure, shear, and torsion, but there has not been much focus on beams where the hollow core is typically placed below the neutral layer of beam. The flexural performance of three hollow core beam specimens was examined in this study and compared with that of a conventional solid beam. The hollow cores were passed longitudinally below the neutral layer of those three specimens with 5%, 10% and 15 % core replacement of cross section The flexure test was conducted over simply supported beam specimens using two-point loading. Flexural stiffness, maximum deflections, crack pattern, ultimate load capacity, and deflection variations with load were all thoroughly investigated. To support the test outcomes, nonlinear finite element analysis was also performed on the same specimens. Both experimental and analytical results indicate that hollow core beams demonstrate flexural behaviour in terms of load-carrying capacity, deflection, stiffness, and failure patterns comparable to that of solid beams.

1 Introduction

The technique of hollow core beam is widely used in bridge girders worldwide; which helps to reduce the dead weight of structures creating the ducts throughout their spans. The same concept can also be used in RC buildings where it is possible to pass the cables and pipelines through the hollow cores longitudinally [1]. This reduces the formation of dead heights caused by the externally placed utility cables and pipelines. This system results into the reduction of concrete weight in beam and increases the effective floor to floor to height for utilization [2].

* *Corresponding author. Tel.: +91 9359235914.*
E-mail address: jsnikam@kkwagh.edu.in

e-ISSN: 2170-127X, (cc) BY-SA

RESEARCH REVIEW of Sciences and Technologies

Several studies have been carried out to assess the structural characteristics of hollow core beams in terms of its flexural, shear and torsional behavior previously. Alnuaimi et al. [3] evaluated the structural behavior of hollow and solid reinforced concrete beams under the various loading configurations like flexure, torsion, and shear. It was discovered that the concrete core contributes to the structural performance of beams and cannot be neglected when bending, shear, and torsion loads are combined. It was recommended to use hollow beam when torsional action is predominant and solid beam when bending moment is dominant. Manikandan et al. [4] observed that by introducing hollow core in tensile zone up to 25% area of the beams, the structural behaviour of beam is not affected in terms of strain, deformations and flexural strength. According to Murugesan et al. [5], hollow RC beams with a longitudinal hole completely below the stress block exhibits more load bearing ability than that of core above the neutral zone. Balaji and Vetturayasudharsanan [6] revealed the fact that the flexural behaviour of hollow core beam was as same as that of solid beam up to 17.5% replacement of core. Abbass et al. [7] discovered that adding 1.5% steel fiber to a hollow core beam increased its load carrying capability by up to 28%. Abbass et al. [8], also evaluated flexural behaviour of hollow core beam with varying size of core and the inclusion of steel fibre. It was observed that the incorporating 1 % steel fibre and 44.4 % core replacement in RC beam does not affect strength, ductility, and toughness comparing with solid beam. In another study of Abbass et al. [9], the flexural behaviour of hollow core beam was evaluated with different fibres with three cross-sectional void ratios of 0.16, 0.28, and 0.44. ECC beams with void ratio of 0.16 and 0.28 were found to have more ductilite than regular beams.

Elamary et al. [10], studied the effect of incorporating the hollow core on flexural response of RCC beam with 3%, 7%, and 10% core area. It was discovered that the hollow core beams exhibited a similar failure pattern, with only about a 5% drop in load-carrying capacity compared with the solid beam. Al-Smadi [11] reported that the decrease in ultimate capacity of hollow beams, relative to a solid beam, is governed by the shape and size of the openings and this reduction can reach up to about 20%. The hollow beam with circular core exhibited higher ductility than hollow beam with square and rectangular shaped core for the same location of hole. Ismael and Hameed [12], concluded that a hollow core with 46 mm diameter is the optimum choice, providing an 11.1% reduction quantity of concrete, with reductions of 13.6% in load at first cracking and 9.3% in ultimate load capacity, respectively. This configuration makes hollow-core self-compacting concrete beams more ductile and allows them to undergo larger deflections before failure. Mansour et al. [2], evaluated the flexural performance of hollow concrete beams with integrated aluminium sections as cores using self-compacting concrete. The results indicated that use of aluminium cores helps to distribute the flexural cracks uniformly along the effective length and delayed the formation of shear cracks, compared with bare hollow specimens having void areas between 16% and 36% cross-section of the beam.

In previous studies, researchers concisely explored the structural characteristics of hollow core beams through practical and theoretical investigations. However, the flexural response of RC beams with hollow cores placed entirely below the neutral axis has not been comprehensively addressed. Most published research focuses on hollow beams with cores passing through or above the neutral axis. Therefore, a detailed investigation of the flexural performance of beams with cores located in the tension zone which exists below the neutral axis is still needed.

2 Experimental Program

The fundamental objective of this research was to investigate at the flexural behaviour of a proposed hollow beam with a core that passes through the cross section below the neutral layer. Hence three specimens (HB40, HB63, HB75) of hollow core beam using PVC pipe as hollow core and one specimen of solid beam (SB) were cast. These specimens were tested for transverse bending at two points and results were compared considering the parameters like flexural strength, maximum deformations, stiffness and crack patterns.

2.1 Details of hollow core and their arrangement

Three PVC circular pipes of diameter 40 mm, 60 mm and 75 mm respectively were used as hollow core. All the specimens were of equal dimensions; the length of beam was 1200 mm with a rectangular cross section of 150 x 200 mm. The same amount of steel was used as main reinforcement at the bottom, anchor bars at the top and stirrups for all specimen, as depicted in Table 1 and Fig. 1.

Table 1 - Specimen Details

Sr. No.	Specimen	Dimensions (mm)	Steel at bottom	Steel at top	stirrups	Diameter of hollow core (mm)	% replacement of core
1	SB	1200 × 150 × 200	2 nos.- 12mm ϕ	2 nos. 8mm ϕ	8mm ϕ @ 300mm c/c	-	0
2	HB40					40	5.3
3	HB63					63	10.4
4	HB75					75	14.7

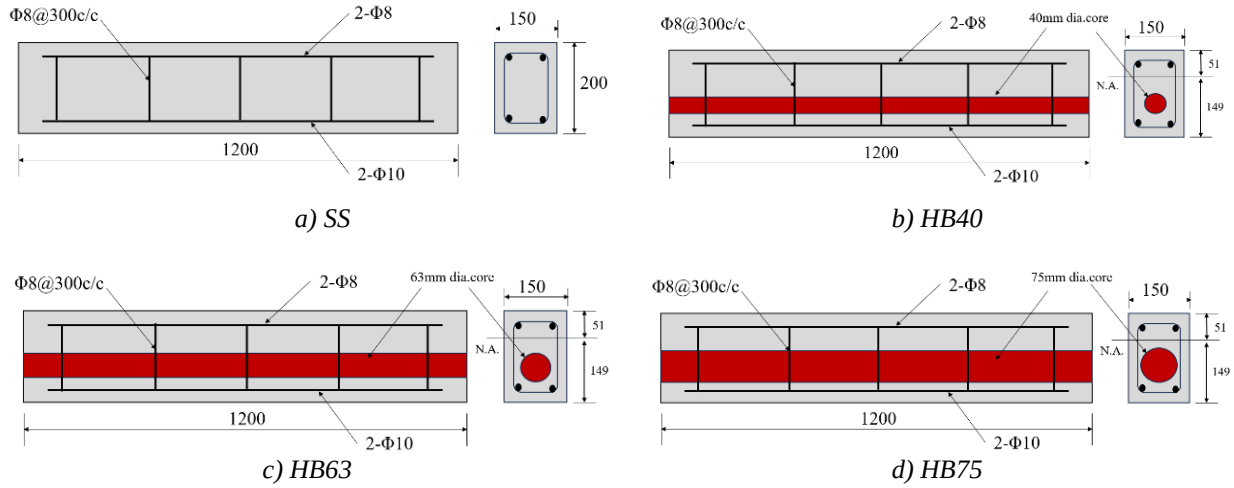


Fig. 1 – Specimen design

2.2 Material Properties

The grade of M25 was used for concrete mix for all specimens. Table 2 shows the mix proportion calculated for M25 grade as per IS10262 [13].

Table 2 – Mix proportions

Cement	439.00 kg/m^3
Water	223.13 kg/m^3
Fine aggregate	673.63 kg/m^3
Coarse aggregate	1027.21 kg/m^3
Free W/C ratio	0.45

Three cubes (150 x 150 x 150 mm) of concrete were made while casting each specimen of beam and cured under the same field conditions as all beam specimens in order to calculate compressive strength of the concrete. Prior to the bending test of the beam specimens, the concrete's compressive strength was calculated (Table 3).

Table 3 – Compressive strength of concrete

Sr No.	Beam	Concrete Mix	Average Compressive Strength (N/mm^2)
1	SB	M25	32.15
2	HB40	M25	31.71
3	HB63	M25	31.69
4	HB75	M25	32.04

The reinforcement was adopted of grade Fe 500 was. Tensile test was conducted to find the mechanical properties of steel which are shown in Table 4.

Table 4 – Properties of steel

Sr No.	Steel Bar Diameter (mm)	Grade	Yield Strength (N/mm^2)	Yield Strain (%)	Ultimate Strength (N/mm^2)
1	8	Fe500	531.0	0.35	640.8
2	12	Fe500	534.0	0.35	671.6

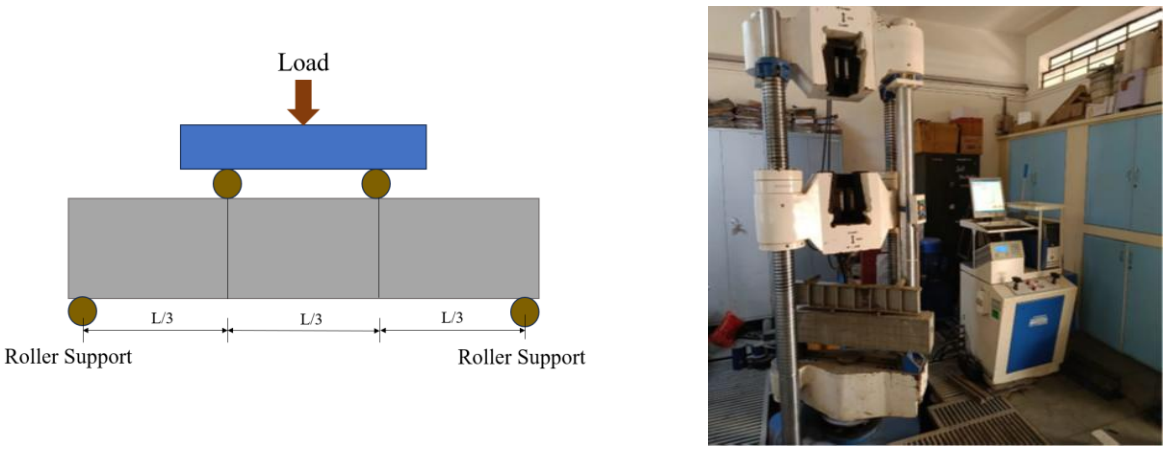
Fig. 2 shows the mould of the beam with the reinforcement arrangement and hollow core before the concreting.



Fig. 2 – Arrangement of hollow core and reinforcement

2.3 Experimental test setup

All beams have been tested in a servo-controlled tension testing machine by positioning them horizontally under two-point loading with a roller situated centrally, as indicated in Fig. 3. A deflectometer was placed at the midpoint of the beam to measure the deflection. The machine exerts a gradually applied load through a steel girder placed over the two equally spaced rollers on the beam. The loads along with their associated deformations were documented, the lines were marked over the cracks at different stages of loading. The load was continued until it reached the maximum load. At that point, the stain in the reinforcement reaches to its maximum value, at this ultimate stage, and the stresses transferred to the concrete in the beam. The loading assembly of the beam is illustrated in the corresponding Fig. 3.



a) Schematic view of setup for flexural test *b) Actual view of two-point loading test setup*

Fig. 3 – Instrumentation and test setup

3 Results and Discussion

Every specimen was tested under two-point loading flexure test. Deflection was recorded at every 1 kN load interval. Also, important observations like formation of cracks, their locations and trend of propagations were noted. Table 5 shows the load at first crack, ultimate load carrying capacity, corresponding deflections, and flexural stiffness.

Table 5 – Experimental Results

Sr. No.	Specimen	Load at First Crack P_{cr} (kN)	Ultimate Load P_u (kN)	Deflection at First Crack δ_{cr} (mm)	Flexural Stiffness K_y (kN/mm)	Maximum Deflection δ (mm)	P_{cr}/P_u
1	SB	47	72	4.26	11.03	7.31	0.65
2	HB40	44	67	4.22	10.43	7.09	0.66
3	HB63	41	61	4.11	9.98	7.32	0.67
4	HB75	39	51	3.96	9.85	8.01	0.76

3.1 Load-deflection behaviour

The load-deflection relationship for all the specimen was illustrated. The crack formations were primarily characterized by the cracks in flexure that extended across the central flexure span. The comparison of load against deflection for solid and hollow beams is presented in Fig. 4**.**

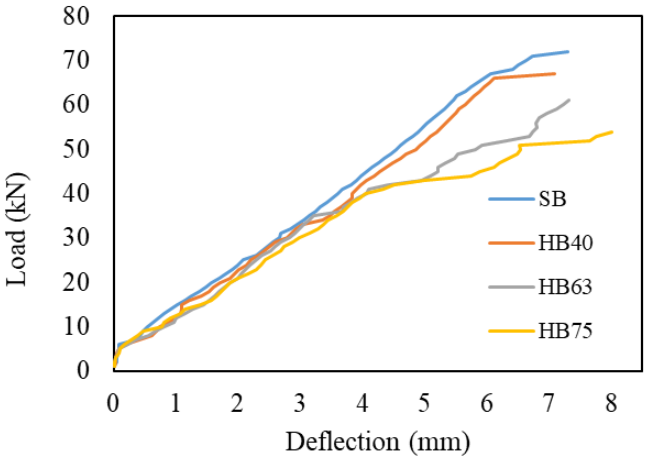


Fig. 4 – Load vs deflection behaviour (experimental study)

At lower load levels, a beam's entire cross-section effectively resists stress, exhibiting a linear relationship between load and deflection. As the load increases, tension-induced cracks emerge at the outer fibres and progress toward the neutral axis. This development disrupts the proportionality between load and deflection, following the inelastic, behaviour. With further loading, the beam reaches its ultimate load-bearing capacity, leading towards the plastic deformations.

The variation in mid-span deflection with gradual increase in load is shown in Fig. 4. In the initial phase, within the elastic state, the load-deflection response is nearly identical for all specimens, indicating that their initial flexural stiffness was almost similar. During this stage, all four beams exhibited similar behaviour, up to the point where flexural cracks began to appear along the bottom surface**.**

Variations in load deflection behaviour begin when the bottom reinforcement yields due to further increases in load. The surface cracks advanced in the direction of the neutral layer. For HB40, HB63, and HB75, the load needed for additional deformation subsequently decreases, which lowers the beam's stiffness. The deviation in a load-deflection curve is caused by the existence of a core, which decreases the net cross section for resisting the stresses which results in more deflection than a solid beam.

3.2 Flexural Stiffness

The flexural stiffness was calculated by taking a ratio of load at first crack (P_{cr}) to corresponding deflection (δ_{cr})

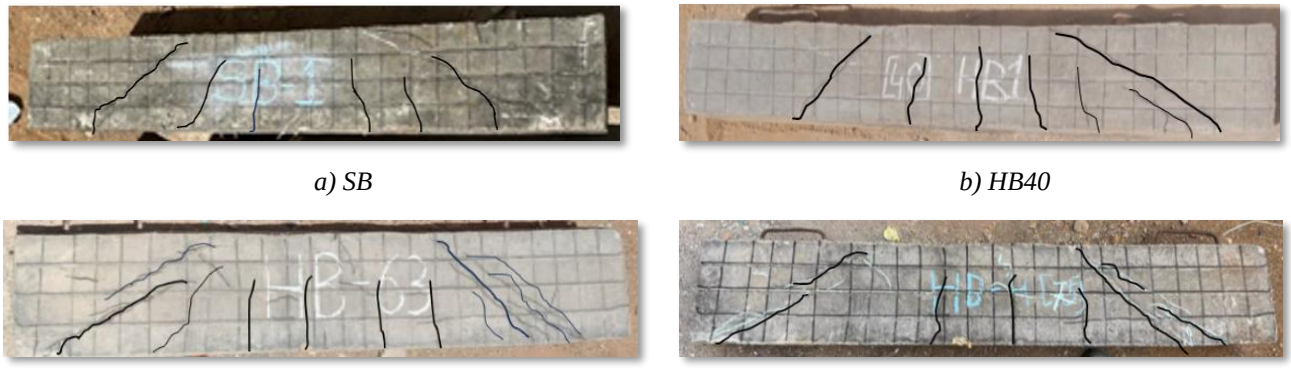
$$K = \frac{P_{cr}}{\delta_{cr}} \quad (1)$$

It was observed that solid beam SB exhibited highest flexural stiffness of 11.03 kN/mm amongst the all the specimens. However, it was decreased by 5.4 % in HB40, 9.5 % in HB63 and 10.7% in HB75. The addition of voids decreases the beam's net cross-sectional area, which lowers the moment of resistance of the section. This causes the hollow core beam's stiffness to decrease. Overall, it was shown that during the elastic loading stage, all hollow core beam specimens showed ductile behaviour comparable to that of solid beam.

3.3 Evaluation of Crack Formations

At the initial stage of loading where cracking was started, fine vertical cracks began to appear in the pure bending span (between the point loads). As the load was increased these cracks propagates continuously, while few of the flexural-shear cracks were started at the same loading levels for beams in addition to these vertical cracks. With the increase in load these cracks propagated from the tension zone to the compression zone extending across the length of beam.

The formation of cracks started firstly in hollow core beam HB75 followed by HB63, HB40 and SB. It was observed that with the increase in core diameter, load at first crack get decreased. For solid slab it was 47 kN, and then it was decreased for HB40 by 6.4 %, for HB63 by 12.8 % and 17% for HB 75. The cause for this drop is the decrease in the effective moment of inertia of beam section. The presence of voids reduces the net cross sectional area of beam which causes the reduction in effective moment of inertia of beam section. Which causes the deduction in the flexural stiffness of the beam. As a whole, it was observed that all the beam specimens followed a pattern of shear-compression failure (where top wedge of concrete tends to crush) pattern since the shear span to depth ratio was 2.15 (between 1 to 2.5). This is basically a combined mode of flexure followed by flexure [14, 15]. Since the nominal reinforcement was provided as stirrups, large diagonal cracks were formed rather than a series of small, distributed cracks. If the shear span to depth ratio would be increased the beam specimen become slender.



a) SB *b) HB40*

c) HB63 *d) HB75*

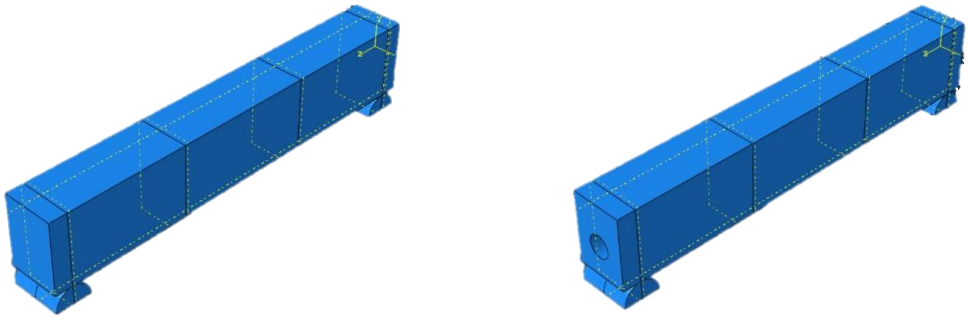
Fig. 5 – Crack Pattern

3.4 Deflection

The deflection at the mid span was measured at every interval of 1 kN loading for all the specimens. Table 5 depicts the deflection at the first crack and deflection at the ultimate stage. The deflection at the first crack was observed to be identical for solid beam specimen and all hollow core beam specimens, which ensures that the initial elastic behaviour of all specimens was almost same. However, it was also seen that all the specimens satisfy the criteria of limiting deflection which is (Le/250=4.4 mm) as per IS 456 [16]. Hollow core beam HB75 deflects maximum amongst all the specimen at the failure stage, however the ultimate deflection for solid beam SB and hollow core beam HB40 and HB63 was very close to each other.

4 Finite element Analysis

ABAQUS dynamic explicit software [17] was adopted to perform a nonlinear finite element analysis (FEA) in order to compare the experimental data and obtain understanding of the complex behaviour of hollow core beams. Different elements of the specimen, namely concrete, longitudinal cores, steel bars and roller supports were prepared in a part section and afterwards placed in the Assembly section depicted in Fig. 6. RCC beam was simulated with three-dimensional deformable solid features and reinforced with two-dimensional deformable wires. Roller support was created as a three-dimensional discrete rigid cylinder part.



a) Solid beam *b) Hollow core beam*

Fig. 6 – Assembly of the FEA model

4.1 Material Modelling

4.1.1 Concrete damage plasticity model (CDPM)

The concrete damage plasticity model has been thoroughly demonstrated in previous research [18–20], which examines crushing of concrete and tensile cracking as potential failure mechanisms. A stress-strain curve in prior research [21, 22] under axial tension and compression of concrete was utilized to simulate concrete behaviour shown in Fig. 7. ABAQUS was able to demonstrate this behaviour for a multi-axial condition. The model is formulated within a plastic-flow framework and combines a non-associated and multi-hardening plasticity law with a scalar damage elasticity formulation to represent stiffness degradation and inelastic deformation of concrete.

Five important factors were used to validate the CDP model in accordance with the guidelines of Alfarah et al. [23]. It was assumed that the eccentricity would be 0.1 and the dilation angle as 31^0 respectively. The ratio of concrete compressive strength in biaxial to that of uniaxial direction $\left({}^{f_{b0}}/_{f_{c0}}\right)$ was determined to be 1.16. Additionally, the ratio of the second stress invariant on the compressive meridian to that on the tensile meridian (K_c), was fixed at 0.7. The parameter of viscosity (μ) was assumed as 0.001.

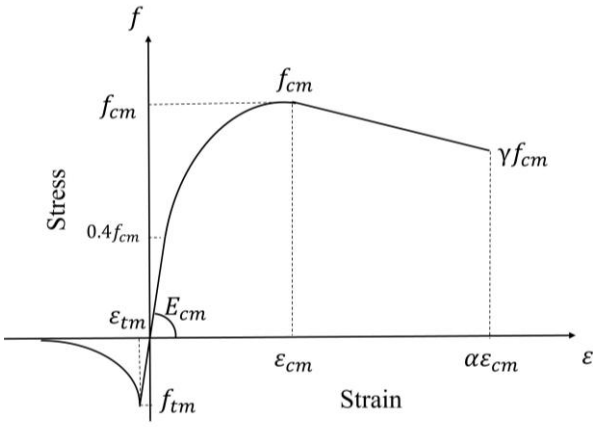


Fig. 7 – Stress-strain relationship of concrete material

The behavior of concrete in compression is depicted in Fig. 7 and can be divided into three distinct sections. The first section exhibits the elastic behavior of concrete up to a limiting stress of $f_o = 0.4f_{cm}$ based on Eurocode 2 specifications [24], where f_{cm} is the concrete's average compressive strength. The value of corresponding strain ε_{cm} with is equal to 0.0022. The Young's modulus was evaluated by applying the formula (Eq. (2)).

$$E_{cm} = 2200\ x\ \left(\frac{f_{cm}}{10}\right)^{0.3} \tag{2}$$

A second section that reaches the maximum value of concrete strength f_{cm}, following the nonlinear parabolic curve derived by the Eq. (3) after the proportional limit.

$$\sigma_c = \left(\frac{kn-n^2}{1+(k-2)n}\right) f_{cm} \tag{3}$$

Where $\begin{cases} n = \frac{\varepsilon_c}{\varepsilon_{cm}} \\ \varepsilon_{cm} = 0.0022\ (the\ strain\ at\ maxmum\ comoressive\ strength) \\ k = 1.1E_{cm}\ x\ \frac{\varepsilon_{cm}}{f_{cm}} \end{cases}$

The last segment of the stress vs strain curve represents the descending branch, beginning at f_{cm} to and extending to a reduced stress level of γf_{cm}, where the the reduction factor γ is defined in study of Ellobody et al. [25]. This factor γ ranges from 1.0 to 0.5 as concrete cube strength increases from 30 to 100 MPa. Drawing from prior work by Nguyen et al. [26], and Khouzani et al. [27], value of γ was fixed as 0.85. Through an iterative series of trials, and by correlating the experimental load–deflection response with the finite-element results, the value of α was established as 5 in this research.

The inelastic deformation ε_c^{In} and plastic deformations ε_c^{pl} are obtained by following Eq. (4) and Eq. (5),

$$\varepsilon_c^{In} = \varepsilon_c - \varepsilon_{0c}^{el} \tag{4}$$

$$\varepsilon_c^{pl} = \varepsilon_c - \varepsilon_c^{el} \tag{5}$$

Where $\begin{cases} \varepsilon_{0c}^{el} = \frac{\sigma_c}{E_0} \\ \varepsilon_c^{el} = \frac{\sigma_c}{E_0}\left(\frac{1}{1-d_c}\right) \end{cases}$

In the tensile response of concrete, the initial portion is modelled as linear elastic until the material reaches its peak tensile strength f_{tm}. Beyond this point, the second stage accounts for tensile damage development, which is described in terms of the crack width, w. The tensile damage of concrete is then expressed through Eq. (6), relating the damage state directly to the evolving crack width [28].

$$\frac{\sigma_t(w)}{f_{tm}} = \left[1 + \left(c_1 \frac{w}{w_c}\right)^3\right] e^{-c_2 \frac{w}{w_c}} - \frac{w}{w_c}(1 + c_1^3) e^{-c_2} \tag{6}$$

The width of crack ranges between w and w_c, where w_c is critical crack width which is equal to $5.14 \times G_f / f_{tm}$; and ε_t and w relation is evaluated by $\varepsilon_t = \varepsilon_{tm} + \frac{w}{l_{eq}}$

In which, $G_f$is fracture energy $0.073 f_{cm}^{0.18}$, $l_{eq}$is the characteristic length and $\varepsilon_{tm} = \frac{f_{tm}}{E_0}$. The cracking strain $\varepsilon_t^{ck}$and plastic strain $\varepsilon_t^{pl}$are calculated by Eq. (7) and Eq. (8)

$$\varepsilon_t^{ck} = \varepsilon_t - \varepsilon_{0t}^{el} \tag{7}$$

$$\varepsilon_t^{pl} = \varepsilon_t - \varepsilon_t^{el} \tag{8}$$

In which, $\begin{cases} \varepsilon_{0t}^{el} = \frac{\sigma_t}{E_0} \\ \varepsilon_t^{el} = \frac{\sigma_t}{E_0}\left(\frac{1}{1-d_t}\right) \end{cases}$

In CDP model concrete degradation is characterised by independent variables like compression damage d_c and tension damage d_t defined by Eq. (9) and Eq. (10).

$$d_c = 1 - \frac{\sigma_c}{f_{cm}} \tag{9}$$

$$d_t = 1 - \frac{\sigma_t}{f_{tm}} \tag{10}$$

Concrete is not damaged when this damage variable is zero, and it is completely damaged when it equals one.

4.1.2 Modelling of Reinforcement

As seen in Fig. 8, referring to earlier research [21] the stress-strain relationship for reinforcing bars was modelled using a bilinear curve.

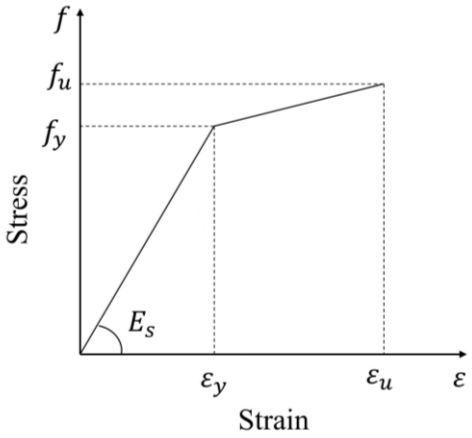


Fig. 8 – Stress-strain relationship of steel reinforcement

4.2 Interactions, Loading and Boundary conditions

The ideal interaction between the concrete and the rebar was ensured by the embedded approach, and there was no slipage steel bar over the concrete surrounded. The bottom surface of the beam and the roller support were found to have a general contact. The normal behaviour was assigned using hard contact and tangential behaviour using penalty friction. To achieve full rigidity, the bottom of a roller support was constrained. To replicate the bending behaviour of the beam, a displacement was introduced at the two equally spaced points in the middle third (Fig. 9).

The steel rebar was modelled with one-dimensional, two-noded truss elements (T3D2). For a concrete a three-dimensional eight-node hexahedral elements (C3D8R) was adopted which comprises a decreased integration technique to prevent shear locking interference [17]. A structured, top-down meshing strategy was employed to manage the mesh and apply the predetermined patterns (Fig. 10). To model the roller support a discrete rigid cylinder was considered. Its meshing was done using four-node, with three-dimensional bilinear rigid quadrilateral elements. The mesh size of 20 mm was used to validate the model following the mesh sensitivity analysis.

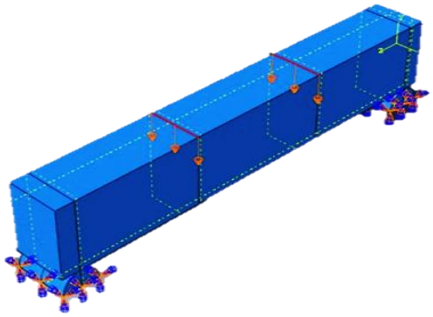


Fig. 9 – Loading and Support Condition

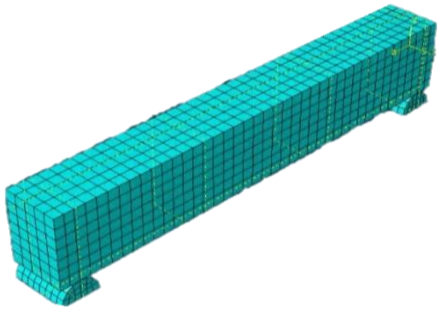


Fig. 10 – Meshing of the specimen

4.3 Results of finite element analysis

The FEA model of the flexure test of a simply supported solid RCC beam and a hollow core beam was simulated using the same loading conditions as in the experiments. To validate this FEA model, the load-deflection curves from experimental tests on specimens SB, HB40, HB63, and HB75 were compared (Fig. 11).

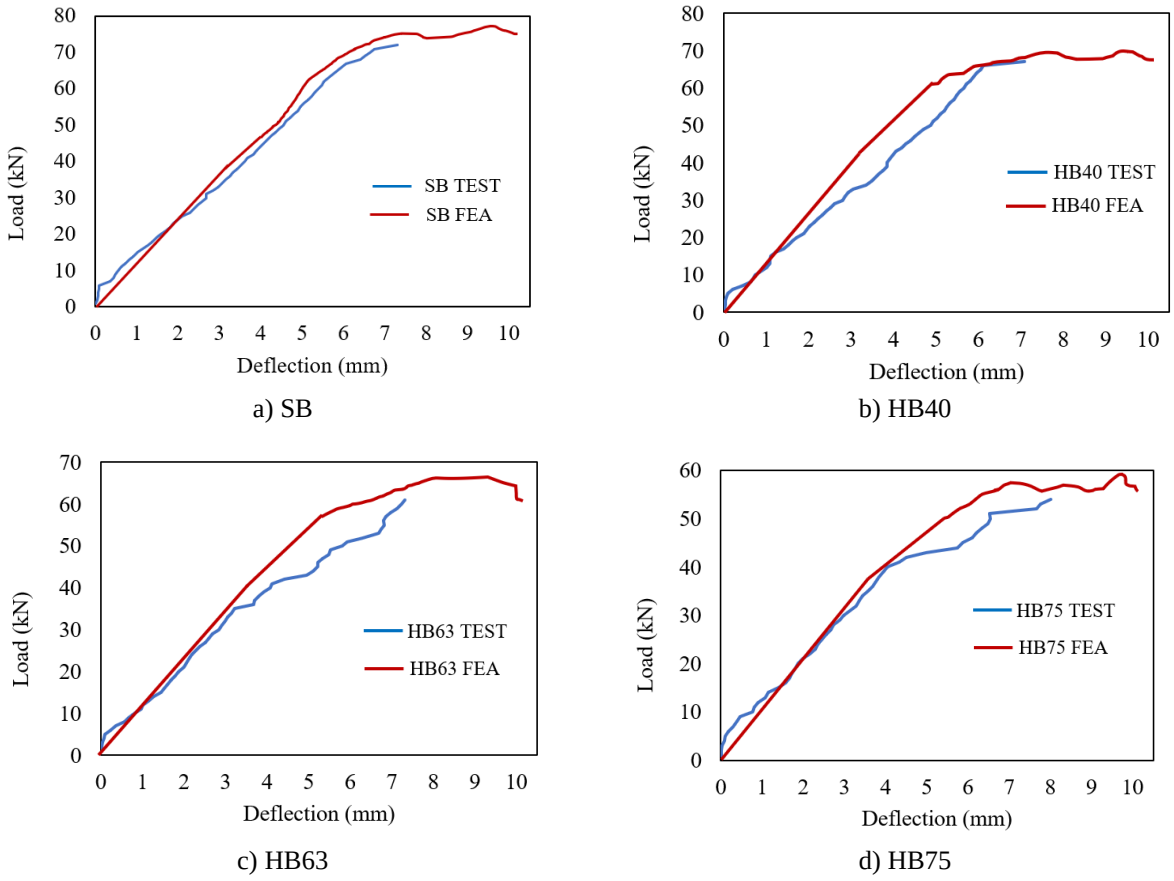


Fig. 11 – Comparison of load vs deflection behaviour by experimental study and FEA

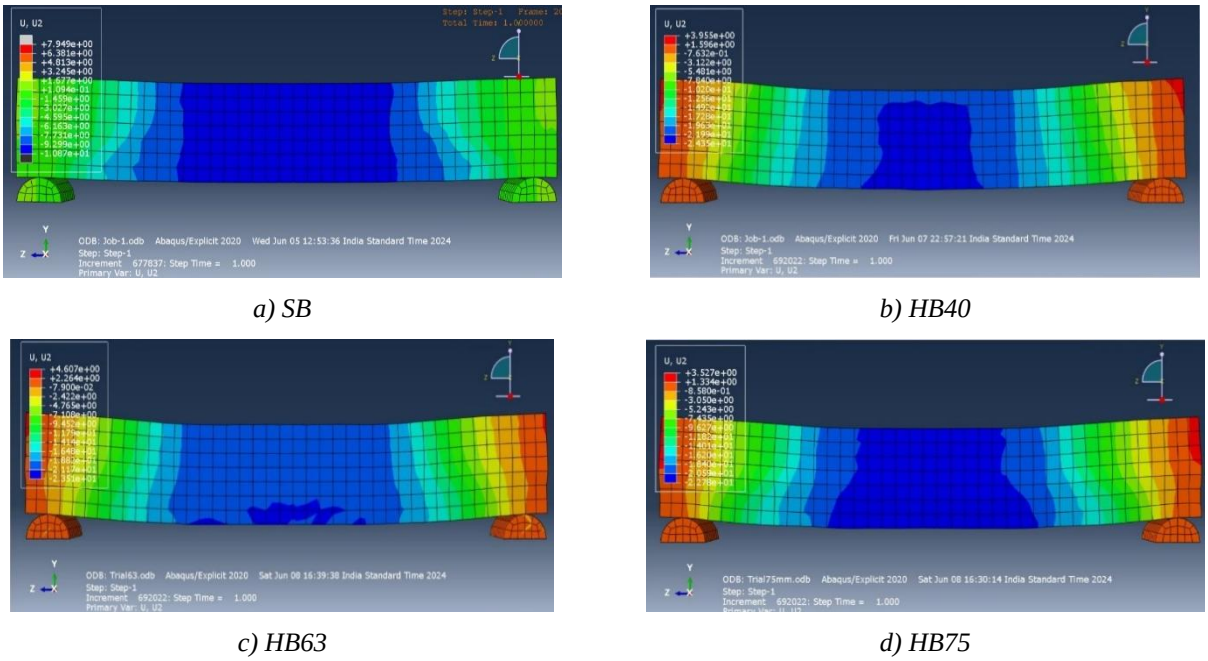
The experimental and numerical load vs. deflection curves at the midspan are almost identical. Furthermore, FEA results for all specimens revealed the flexural behaviour and deformation pattern similar to the test observations. Fig. 12 depicts typical deformed shapes for SB, HB40, HB63, and HB75 specimens.

The described crack patterns (Fig. 13) indicate typical reinforced concrete beam behaviour under loading, with flexural cracks dominating across most specimens (SB, HB40, HB63) and limited shear cracks appearing due to combined bending and shear stresses. Flexural cracks developed primarily from peak tensile stresses in the tension zones near mid-span, while minor shear cracks appeared near the supports in SB, HB40, and HB63 due to dominant diagonal tensile stresses in those regions.

Specimen HB75 uniquely shows pure flexural failure without notable shear cracks, which deviates slightly from experimental results likely expecting some shear involvement at higher loads in contrast, HB75 exhibited pure flexural failure associated with low shear stress levels, which slightly deviates from the experimental results that indicated some shear involvement.

Ultimate load capacity and corresponding deflection was compared with present FEA results are shown in Table 6. The ultimate load capacity by FE analysis results closely matches the test results.

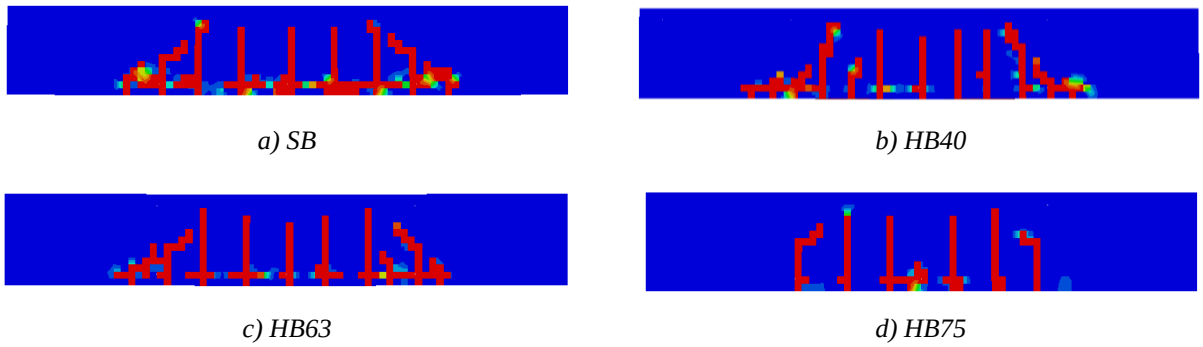
The ratio of ultimate load carrying capacity by test to that of FEA was calculated which was near to 1 for specimen SB, HB40 and HB63. However, it was reported that deflection measured using FEA was quite on higher side than that of test results. It may be because during the experiment for safety of the test setup, experiment was immediately forced to stop at the ultimate stage.



a) SB *b) HB40*

c) HB63 *d) HB75*

Fig. 12 – Deflection Profile



a) SB *b) HB40*

c) HB63 *d) HB75*

Fig. 13 – Crack Distribution by FEA

Table 6 – FEA results

Sr. No.	Beam	Ultimate load Pu (kN)		$P_{u.TEST}/P_{u.FEA}$	Ultimate deflection (mm)	
		FEA	TEST		FEA	TEST
1	SB	77.19	72	0.93	9.09	7.31
2	HB40	70.38	67	0.95	9.23	7.09
3	HB63	66.11	61	0.92	9.57	7.32
4	HB75	59.01	51	0.87	10.03	8.01

5 Conclusion

The flexural performance of hollow core beam was assessed by experimental studies and finite element analysis. Three hollow core beams of varying core sizes and one solid beam has been tested under two-point loading. The flexural behaviour of solid beam was compared with the hollow core beam specimens. Additionally finite element analysis was performed over the 3D model simulating those same specimens. The FEA results were compared to the test results. On this basis, the conclusions are obtained as follows:

1. The failure observed in solid beam was almost same to that of hollow core beams followed by the cracks in flexure propagated vertically and few diagonally.
2. Though solid beam exhibited highest load carrying capacity, hollow core beam specimen HB75 reached upto 71% loading capacity of the solid beam; which offers up to 15 % core replacement of the cross section; however, HB63 exhibited 85 % load carrying capacity with 5% core replacement and HB40 exhibited 94 % load carrying capacity with 10% core replacement.
3. Presence of core reduces net cross sectional area and the effective moment of inertia; thereby reduction in the flexural stiffness of beam. However, the deflection recorded at the first crack are within the limit of serviceability.
4. Numerical investigation of flexural behaviour of hollow core beam performed using finite element analysis confirms the fact that incorporating the core does not affect significantly the flexural characteristics of the beam and exhibited identical behaviour to that of solid beam.

REFERENCES

[1]- H.N.G. Al-Maliki, A. Al-Balhawi, A.J.H. Alshimmeri, B. Zhang, Structural efficiency of hollow reinforced concrete beams subjected to partial uniformly distributed loading. Buildings, 11(9) (2021) 391. https://doi.org/10.3390/buildings11090391
[2]- W. Mansour, U. Ebead, M.T. Nagib, S. Fayed, Behavior of hollow self-compacted concrete beams reinforced with aluminum sections. Structures, 52 (2023) 549-567. https://doi.org/10.1016/j.istruc.2023.04.013
[3]- A.S. Alnuaimi, K.S. Al-Jabri, A. Hago, Comparison between solid and hollow reinforced concrete beams. Mater. Struct., 41(2) (2008) 269-286. https://doi.org/10.1617/s11527-007-9237-x
[4]- S. Manikandan, S. Dharmar, S. Robertravi, Experimental study on flexural behaviour of reinforced concrete hollow core sandwich beams. Int. J. Adv. Res. Sci. Eng., 4(1) (2015) 937-946.
[5]- A. Murugesan, A. Narayanan, Deflection of reinforced concrete beams with longitudinal circular hole. Pract. Period. Struct. Des. Constr., 23(1) (2018) 04017031. https://doi.org/10.1061/(ASCE)SC.1943-5576.0000356
[6]- G. Balaji, R. Vetturayasudharsanan, Experimental investigation on flexural behaviour of RC hollow beams. Mater. Today: Proc., 21 (2020) 351-356. https://doi.org/10.1016/j.matpr.2019.05.461
[7]- A. Abbass, S.R. Abid, M. Özakça, Experimental investigation on the effect of steel fibers on the flexural behavior and ductility of high-strength concrete hollow beams. Adv. Civ. Eng., (2019) 8390345. https://doi.org/10.1155/2019/8390345
[8]- A.A. Abbass, S.R. Abid, F.H. Arna'ot, R.A. Al-Ameri, M. Özakça, Flexural response of hollow high strength concrete beams considering different size reductions. Structures, 23 (2020) 69-86. https://doi.org/10.1016/j.istruc.2019.10.001
[9]- A.A. Abbas, F.H. Arna'Ot, S.R. Abid, M. Özakça, Flexural behavior of ECC hollow beams incorporating different synthetic fibers. Front. Struct. Civ. Eng., 15(2) (2021) 399-411. https://doi.org/10.1007/s11709-021-0701-4
[10]- A.S. Elamary, I.A. Sharaky, M. Alqurashi, Flexural behaviour of hollow concrete beams under three points loading: Experimental and numerical study. Structures, 32 (2021) 1543-1552. https://doi.org/10.1016/j.istruc.2021.03.094
[11]- Y.M. Al-Smadi, N. Al-Huthaifi, A.A. Alkhawaldeh, The effect of longitudinal hole shape and size on the flexural behavior of RC beams. Results Eng., 16 (2022) 100607. https://doi.org/10.1016/j.rineng.2022.100607
[12]- M. Ismael, Y.M. Hameed, Structural behavior of hollow core reinforced self compacting concrete beams. SN Appl. Sci., 4(6) (2022) 178. https://doi.org/10.1007/s42452-022-05036-6
[13]- Bureau of Indian Standards, IS 10262 (2009): Guidelines for concrete mix design proportioning. IS 10262, New Delhi, 2009.
[14]- J.K. Wight, J.G. Macgregor, Reinforced concrete mechanics and design. Pearson, 2009.
[15]- G.N.J. Kani, The riddle of shear failure and its solution. J. Am. Concr. Inst., 61(28) (1964) 441-466.
[16]- Bureau of Indian Standards, IS 456:2000, Plain Concrete and Reinforced. New Dehli, 2000.
[17]- Simulia, ABAQUS/CAE User's Guide. Dassault Systèmes Simulia Corporation, 2014.
[18]- A.S. Genikomsou, M.A. Polak, Finite element analysis of punching shear of concrete slabs using damaged plasticity model in ABAQUS. Eng. Struct., 98 (2015) 38-48. https://doi.org/10.1016/j.engstruct.2015.04.016
[19]- M. Navarro, S. Ivorra, F.B. Varona, Parametric finite element analysis of punching shear behaviour of RC slabs reinforced with bolts. Comput. Struct., 228 (2020) 106147. https://doi.org/10.1016/j.compstruc.2019.106147

[20]- Y.D. Patil, P.A. Singh, R.T. Pardeshi, Experimental and analytical investigation of innovative wing plate headed stud shear connector in composite structures. Structures, 46 (2022) 265-284. https://doi.org/10.1016/j.istruc.2022.10.074

[21]- A.J. Pawar, Y.D. Patil, G.R. Vesmawala, P.D. Dhake, J.S. Nikam, Two-way flexural behavior of biaxial voided slab using cuboidal shape of void formers. Structures, 62 (2024) 106175. https://doi.org/10.1016/j.istruc.2024.106175

[22]- A.J. Pawar, Y.D. Patil, G.R. Vesmawala, P.D. Dhake, J.S. Nikam, Investigating the flexural behaviour of biaxial voided slab with varying size and spacing of cuboidal shaped void formers with innovative type of fixing reinforcement. Structures, 64 (2024) 106616. https://doi.org/10.1016/j.istruc.2024.106616

[23]- B. Alfarah, F. López-Almansa, S. Oller, New methodology for calculating damage variables evolution in Plastic Damage Model for RC structures. Eng. Struct., 132 (2017) 70-86. https://doi.org/10.1016/j.engstruct.2016.11.022

[24]- Eurocode 2, Design of concrete structures - Part 1-1: General rules and rules for buildings, 2004.

[25]- E. Ellobody, B. Young, D. Lam, Behaviour of normal and high strength concrete-filled compact steel tube circular stub columns. J. Constr. Steel Res., 62(7) (2006) 706-715. https://doi.org/10.1016/j.jcsr.2005.11.002

[26]- H.T. Nguyen, S.E. Kim, Finite element modelling of push-out tests for large stud shear connectors. J. Constr. Steel Res., 65(10-11) (2009) 1909-1920. https://doi.org/10.1016/j.jcsr.2009.06.010

[27]- M.A. Khouzani, M. Zeynalian, M. Hashemi, D. Mostofinejad, F. Farahbod, M. Shahadifar, A numerical study on flexural behavior of biaxial voided slabs containing steel cages. J. Build. Eng., 44 (2021) 103382. https://doi.org/10.1016/j.jobe.2021.103382

[28]- K.T.S.R. Iyengar, Two-dimensional theories of anchorage zone stresses in post-tensioned prestressed beams. ACI J. Proc., 59(10) (1962) 1443-1466. https://doi.org/10.14359/7961